Journal of Brilliant Engineering 3 (2025) 41050
Brilliant Engineering
journal home: www.acapublishing.com/journals/4/ben

Research Article

Synthesis and Characterization of BiVO4/WO3/TiO2 Composite for the Photocatalytic Activity of Methylene Blue

Galal Al-siani,[1], Hakan Kiziltas*,[2]
[1,2]Department of Chemical Engineering, Atatürk University, Erzurum, Türkiye

Keywords

Photocatalytic degradation, BiVO4/WO3/TiO2 composite, Methylene blue, Hydrothermal synthesis, Heterojunction.

Abstract

Methylene blue, an organic dye used in dyeing processes in the textile industry, has adverse effects on the ecosystem and human health. The use of catalysts is the most effective method for removing dyes from wastewater. Therefore, in this study, $BiVO_4$, WO_3, and the $BiVO_4/WO_3/TiO_2$ composite were synthesized via hydrothermal methods. The catalysts were characterized using SEM-EDS, XRD, PL, and UV-Vis DRS techniques. XRD diffraction peaks revealed that the synthesized nanoparticles had a monoclinic phase. SEM images confirmed the spherical and rod-like morphology of the samples, while EDS analysis confirmed the presence of oxygen, tungsten, vanadium, bismuth, and titanium elements. PL analysis was performed between 300 and 800 nm to determine the recombination rate of the samples. The band gap values of the samples were determined by UV-Vis DRS analysis. According to the UV-DRS results, the E_g values of $BiVO_4$, WO_3, and the $BiVO_4/WO_3/TiO_2$ composite were determined as 2.38, 2.54, and 2.31 eV, respectively. The photocatalytic activity of the catalysts was investigated by the degradation of methylene blue under UV irradiation. The results showed that $BiVO_4$, WO_3, and $BiVO_4/WO_3/TiO_2$ composites removed 28.02%, 45.10%, and 61.080% of methylene blue dye under UV irradiation, respectively, and the $BiVO_4/WO_3/TiO_2$ composite had a good degradation efficiency.

1. Introduction

The photocatalytic oxidation of water into molecular oxygen under visible light is one of the topics that makes the development of water splitting using solar energy attractive. TiO_2, one of the most commonly used semiconductors in such studies, is attracting considerable attention due to its high photocatalytic activity, stability, and affordability [1]. Therefore, TiO_2 and doped TiO_2 composites are used as photocatalytic materials for dye removal from wastewater under UV light. However, TiO_2 photocatalysts are limited to UV light activation, which limits their practical applications. Various doping processes are required to address this issue and increase visible light activity. [2, 3]. In the study conducted by Zhijia et al., the $BiVO_4/TiO_2$/GO catalyst was synthesized using the solvothermal method. In photocatalytic activity experiments using RB-19 dye, the $BiVO_4/TiO_2$/GO catalyst showed high photocatalytic activity by removing 95.87% of the dye under visible light within 90 minutes [4]. Zhu and co-workers synthesized the $Bi_2S_3/BiVO_4/TiO_2$ ternary photocatalyst and used it to remove methylene orange. They determined that the $Bi_2S_3/BiVO_4/TiO_2$ photocatalyst removed 76.3% of the dye under visible light within 180 min [5]. Therefore, using semiconductor-based composite materials in photocatalytic water oxidation increases the photocatalytic efficiency of semiconductor photocatalysts (PCs) that exhibit water oxidation reactions under visible light. Examples of these semiconductors include photoactive semiconductor metal oxide materials such as ZnO [6], $BiVO_4$ [7], TiO_2 [8], WO_3 [9], and Fe_2O_3 [10, 11]. The efficiency of photocatalysts depends on physicochemical properties such as the stability of the photocatalytic semiconductor material, light absorption rate, catalytic reaction, and charge carrier mobility. Nanostructured and heterojunction materials are being synthesized to improved overall efficiency. To create a heterojunction structure, two materials are needed, and these materials must be matched in band alignment [12].

Bismuth vanadate ($BiVO_4$) is an excellent n-type semiconductor photocatalyst due to its properties, such as photo-responsiveness under visible light for water oxidation reactions with a band gap value of 2.4 eV, absorption at wavelengths up to 520 nm, and a favorable band edge position for oxygen release reactions [13-16]. However, $BiVO_4$ suffers from the disadvantages of a high recombination rate of photogenerated electron-hole pairs and poor charge transport efficiency [17]. Therefore, various approaches, such as cocatalyst loading, doping, and heterojunction formation, are available to overcome the limitations resulting from $BiVO_4$'s poor conductivity [18]. There have been studies on doping $BiVO_4$ photocatalysts with certain metal oxides or metals to improve charge separation efficiency under visible light irradiation. Zhang and co-workers reported that $BiVO_4$ combined with ZnO and Co_3O_4 achieved 99.1% sonophotocatalytic removal of Brilliant green dye [19].

Zou and co-workers used a $BiVO_4$ photocatalyst doped with Zn for the photocatalytic degradation of RhB dye. The $Zn/BiVO_4$ photocatalyst removed 96% of the dye within 90 min [20]. The formation of heterostructures allows for excellent removal of photogenerated electrons, resulting in a reduced recombination rate and increased efficiency. Type II, one of the three different heterostructure formation methods, offers advantages such as rapid mass transfer, a suitable structure for spatial separation of electron-hole pairs, good electron-hole separation efficiency, and a broad spectrum of light absorption [21, 22].

WO_3, an n-type semiconductor, has attracted considerable attention due to its favorable band gap energy, high chemical stability, tunable composition, abundance on earth, and lower conduction band than $BiVO_4$. With a band gap of approximately 2.4-2.8 eV, WO_3 has been incorporated into various semiconductors to reduce electron-hole recombination. The band gap of WO_3 is suitable for absorbing light to generate photoexcited charge carriers, and this metal oxide can utilize 12% of the solar spectrum [3, 23].

*Corresponding Author: h.kiziltas@atauni.edu.tr
Received 01 Aug 2025; Revised 07 Aug 2025; Accepted 07 Aug 2025
https://doi.org/10.36937/ben.2025.41050

In this study, a $BiVO_4/WO_3/TiO_2$ heterojunction structure was synthesized using a hydrothermal method, and its degradation efficiency on Methylene Blue dye was determined. The morphology, crystal structure, and optical properties of the synthesized $BiVO_4/WO_3/TiO_2$ composite were characterized using SEM-EDS, XRD, PL, and UV-Vis DRS instruments.

2. Materials and Method

2.1. Materials

All chemicals used in this study were of analytical grade. Sodium tungstate dihydrate ($Na_2WO_4{\cdot}2H_2O$, Merck), sodium chloride (NaCl, Merck), pH, hydrochloric acid (HCl, 37%, Merck), bismuth(III) nitrate pentahydrate ($Bi(NO_3)_3{\cdot}5H_2O$, 98%, Aldrich), vanadium(V) oxide (V_2O_5, Merck, 99%), potassium sulfate (K_2SO_4, Merck, 99%), (NaOH, Merck, ≥97%), and (TiO_2 P25, Aeroxide®, Degussa) were purchased from the aforementioned companies. Deionized water was used in the entire experimental procedure. Methylene blue ($C_{16}H_{18}ClN_3S$) dye was used for photocatalytic experiments and was purchased from Merck.

2.2. Synthesis of $BiVO_4$

The hydrothermal method was used to synthesize $BiVO_4$. 0.970 g of $Bi(NO_3)_3{\cdot}5H_2O$ (2 mmol), 0.370 g of V_2O_5 (2 mmol), and 10.0 g of K_2SO_4 (0.0574 mol) were dispersed in 100 mL of deionized water with stirring. The mixture was transferred to a Teflon-lined autoclave and kept at 200°C for 24 h. After cooling to room temperature, the solution was filtered, washed, and dried at 80°C. Finally, it was calcined at 550°C for 2 h.

2.3. Synthesis of WO_3

WO3 was synthesized by hydrothermal precipitation. 4.354 g of $Na_2WO_4{\cdot}2H_2O$ (0.0132 mol) and 1.543 g of NaCl (0.0264 mol) were dissolved in 100 mL of deionized water under magnetic stirring. The pH was adjusted to 2 using 3 M HCl. The solution was transferred to a Teflon-lined autoclave reactor and kept at 180 °C for 24 hours. After cooling to room temperature, the solution was filtered, washed, and dried at 80 °C. Finally, it was calcined at 550°C for 2 hours.

2.4. Synthesis of $BiVO_4/WO_3/TiO_2$

1.2 g of $BiVO_4$ and 0.8 g of WO_3 were magnetically stirred in 40 mL of deionized water. The pH was adjusted to 7 using a 0.15 M NaOH solution. On the other hand, 40 mg of P25 was added to 25 mL of deionized water and added dropwise to the main suspension with continuous stirring. The final mixture was transferred to a Teflon-lined reactor and subjected to hydrothermal treatment at 120°C for 6 h. After cooling to room temperature, the solution was filtered, washed, and dried at 80°C. The purpose of the synthesis procedure of the $BiVO_4/WO_3/TiO_2$ composite is to manage the morphology and crystal structure by adjusting the synthesis time, composition of the sample mixture, and temperature.

2.5. Characterization

The crystal structure, morphological, and optical properties of the synthesized materials were characterized using standard techniques. X-ray diffraction (XRD) was used to analyze the crystalline phases of WO_3, $BiVO_4$, and the $BiVO_4/WO_3/TiO_2$ composite. To determine the crystal structure, a wavelength between 10-90° (λ = 1.5406Å) was used. Scanning electron microscopy (SEM-EDS) was used to investigate the surface morphology and elemental distribution. Photoluminescence (PL) analysis was performed to evaluate the recombination behavior of photoinduced charge carriers. Additionally, UV-Vis diffuse reflectance spectroscopy (UV-Vis DRS) was used to determine the optical absorption properties of the samples and to estimate their band gap energies.

2.6. Photocatalytic activity experiments on Methylene Blue

The photocatalytic activity of the prepared samples $BiVO_4$, WO_3, and the $BiVO_4/WO_3/TiO_2$ composite was investigated through the degradation of methylene blue (MB) dye under light irradiation. The initial concentration of MB was set to 10 ppm, and 400 mL of this dye solution was used in each experiment. 100 mg of the photocatalyst sample was added and dispersed thoroughly using magnetic stirring. To establish adsorption–desorption equilibrium between the dye molecules and the catalyst surface, the suspension was stirred in the dark for 5 minutes prior to illumination. A low-pressure mercury vapor UV lamp (UV-C region) with a light intensity of 44 W/m^2 and a wavelength of 254 nm was employed as the UV light source. Continuous air flow was provided using a laboratory air pump throughout the experiment to ensure sufficient oxygen availability. To determine the dye concentration, 3 ml of sample was withdrawn at certain intervals and the concentration value was determined at 665 nm in UV spectroscopy.

3. Result and Discussion

3.1. Morphological characterization and X-ray diffraction

SEM-EDS images of $BiVO_4$, WO_3, and the $BiVO_4/WO_3/TiO_2$ composite are shown in Figure 1.

The SEM image of the $BiVO_4$ nanoparticles shown in Figure 1a shows that the nanoparticles synthesized using the hydrothermal method have a rod-like morphology [24]. Adding K_2SO_4 during the synthesis process facilitated the separation of the $BiVO_4$ nanoparticles by centrifugation. Furthermore, the addition of K_2SO_4 appears to have resulted in the formation of rod and nanoparticle structures. Adding K_2SO_4 to the hydrothermal synthesis of $BiVO_4$ improves particle morphology. The presence of K_2SO_4 positively influences the synthesis, leading to the formation of spherical and rod-like $BiVO_4$ particles with a more uniform shape. Figure 1b shows the SEM image of WO_3 nanoparticles synthesized via the hydrothermal method. WO_3 appears to have a plate-like and particle-shaped morphology. The different sizes of the particles indicate that agglomeration has occurred [25]. Figure 3c illustrates the SEM image of the $BiVO_4/WO_3/TiO_2$ composite. The SEM images reveal that TiO_2 nanoparticles surround the $BiVO_4/WO_3$ structure. Although the presence of $BiVO_4$ is not clearly visible in the SEM images, TiO_2 particles are distinctly adhered to the WO_3 structure [26]. The EDS plot also indicates that $BiVO_4$ is partially covered by WO_3 nanoparticles. EDS analysis confirms the presence of oxygen, vanadium, bismuth, tungsten, and titanium within the structure.

Figure 2 shows the XRD graphs of $BiVO_4$, WO_3, and $BiVO_4/WO_3/TiO_2$ composites.

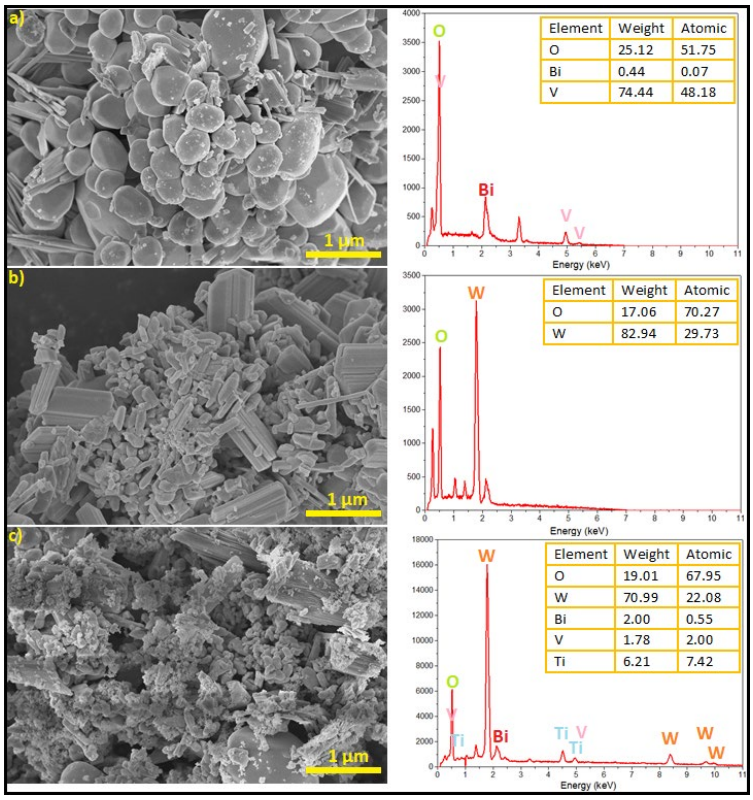

Figure 1. SEM and Energy Dispersive Spectra of synthesized of $BiVO_4$, WO_3, and $BiVO_4/WO_3/TiO_2$ composite

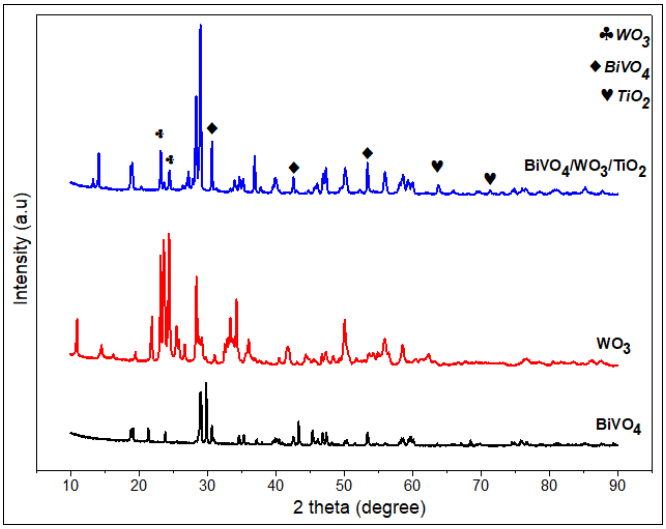

Figure 2. Powder X-ray diffraction of synthesized $BiVO_4$, WO_3, and $BiVO_4/WO_3/TiO_2$ composite

The diffraction peaks observed in the XRD graph correspond to the monoclinic phase of $BiVO_4$. It is assumed that vanadium is a major source of the formation of homogeneous $BiVO_4$ particles. Monoclinic $BiVO_4$ nanoparticles (JCPDS No. 75-2480) are observed to be fully compatible.

Precipitation of WO_3 nanoparticles synthesized via the hydrothermal method is expected due to the chemicals used during the process. XRD analysis determined that the nanoparticles calcined at 550°C exhibited a crystalline form. The WO_3 nanoparticles appear to have a monoclinic structure and comply with (JCPDS No. 43-1035). In the hydrothermal process starting from $Bi(NO_3)_3{\cdot}5H_2O$ and $Na_2WO_4{\cdot}2H_2O$, the time and temperature parameters were determined to ensure the conversion of these starting materials into metal oxides. In the XRD diagram of the $BiVO_4/WO_3/TiO_2$ composite, the diffraction peaks of WO_3 at 23.17° and 24.3° correspond to the (002) and (200) planes, respectively. $BiVO_4$ exhibits diffraction peaks at 30.7, 42.7, and 53.4°. Although the TiO_2 peak intensity is quite difficult to see compared to the other samples, these diffraction peaks conform to the crystal structure of heterostructured anatase TiO_2.

3.2. PL and UV-Vis-DRS analysis

To investigate the recombination of electron-hole pairs in composites with semiconductor heterostructures, photoluminescence (PL) analysis was performed. Figure 3 shows the PL spectra of $BiVO_4$, WO_3, and the $BiVO_4/WO_3/TiO_2$ composite with excitation source wavelengths of 325 nm. The PL intensity of the $BiVO_4/WO_3/TiO_2$ structure is observed to be lower than that of $BiVO_4$ and WO_3 [27].

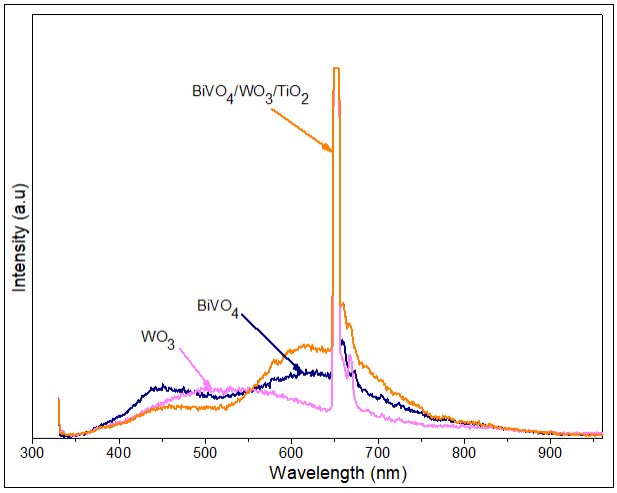

Figure 3. PL spectrum of the $BiVO_4$, WO_3, and $BiVO_4/WO_3/TiO_2$ composite

The room temperature PL spectrum of WO_3 nanoparticles shows a sharp line between 647 and 656 nm. The room-temperature PL spectrum reveals that WO_3 has lower intensity than $BiVO_4$ in the peaks observed between 450 and 550 nm, indicating that WO_3's photocatalytic activity is superior to $BiVO_4$. When excited at 325 nm, prominent peaks show a sharp line at 647 and 656 nm. This characteristic line can be attributed to emission from one band to another caused by quantum confinement effects within the structure. The small PL peak at 430 nm corresponds to WO3, and the small PL peak observed at 460 nm corresponds to emission near the band edges of $BiVO_4$. Oxygen clustering in the structures is attributed to the recombination of vacancies and oxygen-induced defects in the alloys. Because the $BiVO_4/WO_3/TiO_2$ composite significantly reduces the recombination time of photogenerated carriers, the room temperature PL spectrum of the composite is low-intensity, indicating efficient separation of electrons and holes within the composite. Photocatalytic results confirm the photocatalytic removal of Methylene blue under UV irradiation. The weak PL intensity of the $BiVO_4/WO_3/TiO_2$ composite suggests that this ternary structure plays an important role in separating the photogenerated charge and inhibiting the recombination of electron-hole pairs, improving the photocatalytic activity of the catalytic composite material.

UV–Vis DRS spectrophotometer results of $BiVO_4$, WO_3, and $BiVO_4/WO_3/TiO_2$ composites are shown in Figure 4. To determine the estimated band gaps of the composites, spectra were recorded using diffuse reflectance mode at wavelengths of 300–800 nm. To estimate the band gap energy of $BiVO_4$ and WO_3 nanoparticles and $BiVO_4/WO_3/TiO_2$ composite structures annealed at 550 °C, it was calculated using Tauc plots and the Kubelka-Munk (K-M) formula as shown in Figure 4. The optical band gaps of $BiVO_4$, WO_3 and $BiVO_4/WO_3/TiO_2$ composites were calculated along with the Tauc plots as given in Equation 1.

$$\alpha h\vartheta = A(h\vartheta - Eg)^n \quad (1)$$

Where all parameters have a meaning and the exponent n depends on the type of transition. For the indirect band gap, n = 2 is used, while for the direct band gap, n = 0.5 is used. Studies have shown that $BiVO_4$ (n=1/2) [28] has a direct band gap and WO_3 (n=2) [29] has an indirect band gap. A is the disorder parameter constant, E_g is the optical energy of the composites, $h\vartheta$ (eV) is the energy of the photon, and α(cm^{-1}) is the absorption coefficient. The optical band gap energy of the composites was estimated by a linear fit of $h\vartheta$ $(h\vartheta\alpha)^{0.5}$ against. Accordingly, the optical bandgap energies of $BiVO_4$, WO_3, and $BiVO_4/WO_3/TiO_2$ composites were obtained as 2.38, 2.54, and 2.31 eV, respectively.

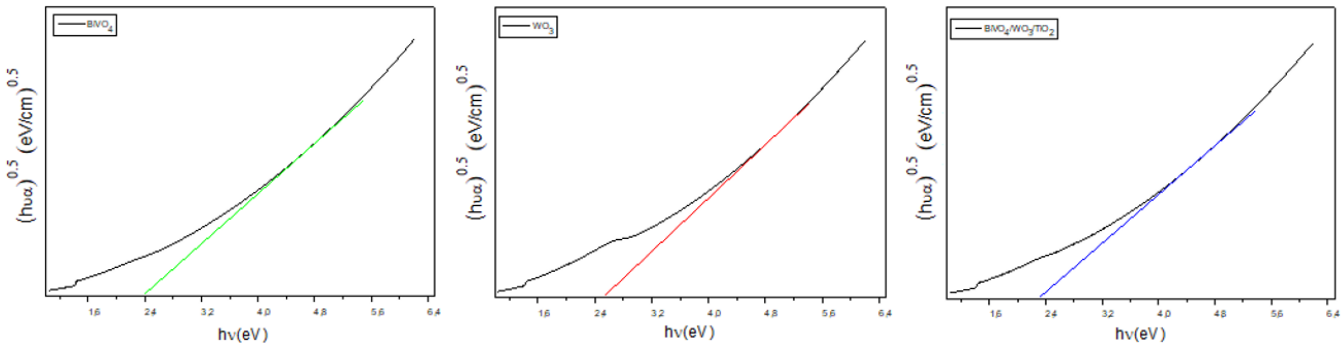

Figure 4. Optical bandgap of $BiVO_4$, WO_3, and $BiVO_4/WO_3/TiO_2$ composites

3.3. Determination of photocatalytic activity on Methylene Blue

The degradation graph shown in Figure 5 shows the photocatalytic activity of $BiVO_4$, WO_3, and the $BiVO_4/WO_3/TiO_2$ composite on methylene blue under UV irradiation. According to the degradation graph, when comparing $BiVO_4$, WO_3, and $BiVO_4/WO_3/TiO_2$ samples, it is clearly seen that the ternary heterostructure exhibits superior photocatalytic activity.

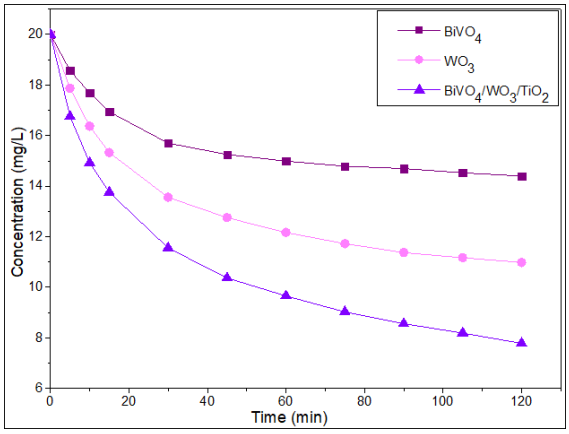

Figure 5. Photocatalytic degradation graph of the $BiVO_4$, WO_3, and $BiVO_4/WO_3/TiO_2$ composite in Methylene blue

The $BiVO_4$ photocatalyst used alone demonstrated the lowest efficiency in degrading MB molecules. This is believed to be due to $BiVO_4$'s low catalytic efficiency despite its narrow band gap, rapid electron-hole recombination, and limited surface activity. $BiVO_4$ nanoparticles were found to remove 28.02% of the dye. Bismuth vanadate is oxygen-deficient, and oxygen in aqueous solution readily generates oxygen species such as O^-, O^{-2}, and O_2^{-2} using electrons on the catalyst surface. The holes in the valence band react with water or hydroxyl groups to produce H_2O. Furthermore, degradation occurs through reaction with methylene blue. The low dye removal efficiency of $BiVO_4$ is thought to be due to the amount of catalyst and the degradation being carried out under UV light. $BiVO_4$ exhibited lower activity because an increase in catalyst loading resulted in a decrease in the formation of active species, which in turn resulted in less light scattering. The photocatalytic activity of metal oxides depends on many parameters, such as crystal size, morphology, surface-to-volume ratio, and lattice defects. The monoclinic structure, plate-like morphology, and annealing temperature of WO_3 particles are ideal for the photocatalytic activity of the synthesized WO_3 particles. Annealing at 550°C yielded a well-crystallized monoclinic phase and improved photocatalytic activity. Literature studies indicate that annealing at 600°C yields the highest photocatalytic activity [30]. On the other hand, the WO_3 catalyst offered a better degradation rate compared to $BiVO_4$, but it still fell short of the optimum level. Despite WO_3's high oxidation potential, the valence and conduction band positions alone are insufficient for effective charge transport. WO_3 nanoparticles removed 45.10% of the dye. The most striking result was obtained with the three-component $BiVO_4/WO_3/TiO_2$ heterostructure. The rapid decrease in MB concentration over time indicates that this structure provides more efficient photoassisted charge separation and enhances the formation of reactive species. The multiple heterojunctions in this structure facilitate the conduction of electrons generated after photoexcitation and prevent hole recombination. Furthermore, the large surface area and improved light absorption also contribute to the photodegradation capacity of this system. The $BiVO_4/WO_3/TiO_2$ composite removed 61.080% of the dye.

As shown in Figure 6, to examine the effect of the pollutant on the degradation process, KI, BQ, and $KBrO_3$, inorganic scavengers, and IPA, an organic scavenger, were added to the solution medium. The oxidation reaction of the $BiVO_4/WO_3/TiO_2$ composite was carried out using UV light.

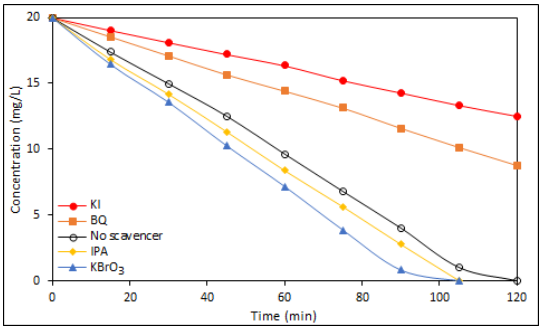

Figure 6. The effect of scavengers on the photocatalytic oxidation process of Methylene blue dyestuff on $BiVO_4/WO_3/TiO_2$ composite

According to the test results, the addition of $KBrO_3$, an inorganic scavenger, did not alter the oxidation process. The addition of BQ, another inorganic scavenger, caused a change, while the addition of KI, an inorganic scavenger, caused blockages in the photocatalytic oxidation reaction. The addition of IPA, an organic scavenger, did not alter the oxidation reaction process. This suggests that pores are the primary catalyst in the photocatalytic oxidation process, with oxygen peroxide radicals serving as the primary active species.

4. Conclusion

In summary, $BiVO_4$, WO_3, and $BiVO_4/WO_3/TiO_2$ composites were successfully studied using the hydrothermal method. XRD results confirmed the monoclinic structure of $BiVO_4$ and WO_3. SEM results verified the rod-like and spherical morphologies of the synthesized samples. In PL studies, a strong emission peak at 656 nm was observed. UV-Vis DRS results showed that the Eg values of $BiVO_4$, WO_3, and the $BiVO_4/WO_3/TiO_2$ composite were 2.38, 2.54, and 2.31 eV, respectively. The $BiVO_4/WO_3/TiO_2$ composite demonstrated good photocatalytic activity with a degradation percentage of 61.080%. The band gap of 2.31 eV for the $BiVO_4/WO_3/TiO_2$ composite indicates a slow recombination rate of electron-hole pairs and suggests it is a promising photocatalyst for dye removal under UV light.

Declaration of Conflict of Interests

The authors declare that there is no conflict of interest. They have no known competing financial interests or personal relationships that could have appeared to influence the work reported in this paper.

References

[1.] Yu, J.M., et al., High-performance and stable photoelectrochemical water splitting cell with organic-photoactive-layer-based photoanode. 2020. 11(1): p. 5509.

[2.] Xu, C., et al., Nanotube enhanced photoresponse of carbon modified (CM)-n-TiO2 for efficient water splitting. 2007. 91(10): p. 938-943.

[3.] Chatchai, P., et al., Efficient photocatalytic activity of water oxidation over WO3/BiVO4 composite under visible light irradiation. 2009. 54(3): p. 1147-1152.

[4.] [Zhu, Z., et al., A novel pn heterojunction of BiVO4/TiO2/GO composite for enhanced visible-light-driven photocatalytic activity. 2017. 209: p. 379-383.

[5.] Liu, Z., et al., In-situ preparation of double Z-scheme Bi2S3/BiVO4/TiO2 ternary photocatalysts for enhanced photoelectrochemical and photocatalytic performance. 2021. 545: p. 148986.

[6.] Abdullah, R., et al., Recent advances in zinc oxide-based photoanodes for photoelectrochemical water splitting. 2025. 107: p. 183-207.

[7.] Fu, L., Z. Li, and X.J.I.J.o.H.E. Shang, Recent surficial modification strategies on BiVO4 based photoanodes for photoelectrochemical water splitting enhancement. 2024. 55: p. 611-624.

[8.] Sawal, M., et al., A review of recent modification strategies of TiO2-based photoanodes for efficient photoelectrochemical water splitting performance. 2023. 467: p. 143142.

[9.] Kumbhar, V.S., et al., Enhanced photoelectrochemical water splitting with WO3/TiO2 core/shell heterojunction photoanodes: Unveiling the role of dendritic TiO2. 2025. 142: p. 159-167.

[10.] Fu, W., et al., Progress in promising semiconductor materials for efficient photoelectrocatalytic hydrogen production. 2024. 29(2): p. 289.

[11.] Rokade, A., et al., Realization of electrochemically grown a-Fe2O3 thin films for photoelectrochemical water splitting application. 2021. 17: p. 242-255.

[12.] Wang, G., et al., Advancements in heterojunction, cocatalyst, defect and morphology engineering of semiconductor oxide photocatalysts. 2024. 10(2): p. 315-338.

[13.] Wahba, M.A.J.O.M., Visible-light responsive BiVO4 nanocompositions: Enhanced photocatalytic, electrical and optical performance through Ni and Ni/Co doping. 2024. 147: p. 114643.

[14.] Sánchez-Albores, R., et al., Characterization and photoelectrochemical evaluation of BiVO4 films developed by thermal oxidation of metallic Bi films electrodeposited. 2023. 153: p. 107184.

[15.] Kalanoor, B.S., H. Seo, and S.S.J.M.S.f.E.T. Kalanur, Recent developments in photoelectrochemical water-splitting using WO3/BiVO4 heterojunction photoanode: A review. 2018. 1(1): p. 49-62.

[16.] Yuan, M., et al., Carrier confinement activated explicit solvent dynamic of CdS/BiVO4/H2O and optimized photocatalytic hydrogen evolution performances. 2024. 658: p. 571-583.

[17.] Geronimo, L., et al., Understanding the internal conversion efficiency of BiVO4/SnO2 photoanodes for solar water splitting: An experimental and computational analysis. 2024. 7(5): p. 1792-1801.

[18.] Kamble, G.S., et al., BiVO4 as a sustainable and emerging photocatalyst: Synthesis methodologies, engineering properties, and its volatile organic compounds degradation efficiency. 2023. 13(9): p. 1528.

[19.] Zhang, J. and L.J.C.P.L. Xie, Synthesis and sonophotocatalytic activities of ZnO\BiVO4\Co3O4 composites. 2021. 775: p. 138660.

[20.] Zou, Y., et al., Hydrothermal synthesis of Zn-doped BiVO4 with mixed crystal phase for enhanced photocatalytic activity. 2021. 119: p. 111398.

[21.] Yang, H.J.M.R.B., A short review on heterojunction photocatalysts: Carrier transfer behavior and photocatalytic mechanisms. 2021. 142: p. 111406.

[22.] Low, J., et al., Heterojunction photocatalysts. 2017. 29(20): p. 1601694.

[23.] Nomellini, C., et al., Improved photoelectrochemical performance of WO3/BiVO4 heterojunction photoanodes via WO3 nanostructuring. 2023. 15(45): p. 52436-52447.

[24.] Zhou, Y., et al., An inorganic hydrothermal route to photocatalytically active bismuth vanadate. 2010. 375(1): p. 140-148.

[25.] Antony, A.J., et al., Enhancing the visible light induced photocatalytic properties of WO3 nanoparticles by doping with vanadium. 2021. 157: p. 110169.

[26.] Kyaw, A.M.M., et al., Fabrication and characterization of heterostructure WO3/BiVO4/TiO2 photocatalyst for efficient performance of photoelectrochemical water splitting. 2025. 72: p. 87-92.

[27.] Sajid, M.M., T.J.A.J.f.S. Alomayri, and Engineering, Synthesis of TiO2/BiVO4 Composite and Cogitation the Interfacial Charge Transportation for Evaluation of Photocatalytic Activity. 2023. 48(1): p. 883-891.

[28.] Xu, H., et al., Preparation, characterization and photocatalytic activity of transition metal-loaded BiVO4. 2008. 147(1): p. 52-56.

[29.] Baishya, K., et al., Graphene-mediated band gap engineering of WO3 nanoparticle and a relook at Tauc equation for band gap evaluation. 2018. 124(10): p. 704.

[30.] Thilagavathi, T., et al., An investigation on microstructural, morphological, optical, photoluminescence and photocatalytic activity of WO3 for photocatalysis applications: an effect of annealing. 2021. 31(3): p. 1217-1230.

How to Cite This Article

Al-siani, G., and Kiziltas, H., Synthesis and Characterization of BiVO4/WO3/TiO2 Composite for the Photocatalytic Activity of Methylene Blue. Brilliant Engineering 3(2025), 41050.
https://doi.org/10.36937/ben.2025.41050